J. Fluid Mech. (1986), *vol.* 171, *pp.* 339–363
Printed in Great Britain

The response of an incompressible, viscoelastic coating to pressure fluctuations in a turbulent boundary layer

By JAMES H. DUNCAN

Flow Research Company, 1320 Fenwick Lane, Suite 401, Silver Spring, MD 20910, USA

(Received 11 November 1985 and in revised form 10 April 1986)

The response of the interface between a compliant surface and a turbulent boundary-layer flow is examined theoretically. This response is forced by transient, convected, interfacial pressure pulses that represent the footprints of turbulent flow structures in the boundary layer. Calculations are presented for coatings with a wide range of damping and densities equal to the density of the flow. For coatings with moderate damping, three regimes of response are found. When the flow speed U_∞ is less than about 1.2 (non-dimensionalized by the shear wave speed of the coating), the response is stable and primarily localized under the pressure pulse. For flow speeds from 1.2 to as high as 2.8, depending on the damping, the response is also stable, but it includes a wave pattern behind the pressure pulses. For flow speeds above 2.8, the response is unstable and eventually forms a two-dimensional wavetrain moving in the flow direction. At the highest stable flow velocity, the amplitude of the surface displacements reaches 4.0% of the boundary-layer displacement thickness δ^* and the energy transfer from the pressure pulse reaches $5.0 \times 10^{-4}\, U_\infty^2 (\delta^*)^2$. For high damping, the coating response is again stable when the flow speed is below 2.8. However, there is no wavelike response regime; the path that is traversed by the pressure pulse is covered by a scar that heals according to the viscous relaxation properties of the material. The amplitude of the response is at most $0.01\delta^*$.

1. Introduction

A number of investigators have attempted to design a compliant layer that can reduce skin friction when placed between a rigid surface and a turbulent boundary-layer flow. This work has been reviewed by Bushnell, Hefner & Ash (1976) and more recently by Gad-el-Hak (1986*b*). In order to achieve the desired reductions, the proposed compliant layer must alter the behaviour of turbulent flow structures by deforming in response to the unsteady pressures and shear stresses imposed on its surface by the flow structures themselves. This response can be stable or unstable. For single-layer, homogeneous, incompressible, isotropic coatings under turbulent boundary-layer flows, instabilities occur when the ratio of the dynamic pressure of the flow divided by the shear strength of the coating $\rho_c C_t^2$ (where ρ_c is the coating density and C_t is the shear wave speed of the coating) reaches a critical value (Duncan, Waxman & Tulin 1985). The critical value depends on the damping in the coating, the ratio of the coating thickness to the boundary-layer thickness, and the Reynolds number of the flow. For coatings with high damping these instabilities have been studied experimentally by Gad-el-Hak, Blackwelder & Riley (1984), Hansen & Hunston (1983), and Hansen *et al.* (1979). The theory of Duncan *et al.* (1985)

evaluated at high damping compares well with the experimental results. Instabilities have also been explored experimentally for coatings with low damping (Gad-el-Hak 1986*a*). No theoretical results have been reported in this case. In the presence of instabilities, the surface is dominated by two-dimensional, large-amplitude waves which will most certainly alter the turbulent boundary layer. However, experiments with compliant coatings (A. D. Rathsam 1985, private communication; Hansen & Hunston 1983) and experiments and numerical calculations with moving wavy walls (Kendall 1970; Lin, Walsh & Balasubramanian 1984; Sengupta & Lekoudis 1985) have shown that these organized wave motions increase the surface drag when moving at typical wave speeds. The presence of these large-amplitude waves also masks the smaller-amplitude, local response of the surface to individual turbulent flow structures.

In the present paper, the response of the coating to individual turbulent flow structures (for example turbulent bursts) is examined under stable conditions. In order to analyse the full problem, one would need accurate models of the dynamics of turbulent flow structures, the dynamics of complex viscoelastic materials, and the coupling between the fluid and the solid. The most complete method to investigate this problem would be a large-eddy simulation with a compliant wall. However, it is advantageous to gain some physical insight into the problem before undertaking the expense and time of large-eddy simulations. To this end, a simplified, two-dimensional, quasi-interactive problem has been examined in this paper using a model where a translating, unsteady pressure pulse is imposed on the upper surface of a layer of incompressible Voigt material. The material is attached to a rigid surface on its lower side and is bounded by a potential flow, representing the mean boundary-layer flow, on the other. Thus, the model allows for a full interaction between the coating and the mean flow, but only a one way interaction between the imposed pressure distribution and the coating. This approach is similar to that used in spectral theories of flow-induced vibrations of panels (Dowell 1975). In order to relate the problem to turbulent flows, the characteristics of the pressure pulses are taken from measurements with turbulent flows over rigid walls (Willmarth 1975), and the potential flow is modified to incorporate the reduced magnitudes and phase shifts found experimentally in boundary-layer flows over moving wavy walls (Kendall 1970). This model is used first to calculate the dispersion curves for elemental waves on the interface. From the dispersion curves, the range of stable flow speeds is determined as a function of the stiffness, damping and thickness of the coating. Within the stable range of parameters the response of the coating is examined. In particular, the general shape and amplitude of the response and the energy transfer to the flow–coating system are calculated. The dispersion curves are also used in a quasi-steady theory to compute the lines of constant phase for the three-dimensional problem.

2. Theoretical analysis

2.1. *Statement of the problem*

The coating is modelled as a layer of homogeneous, isotropic, Voigt material. On its lower surface ($y = -d$) the coating is attached to a rigid plate, while on its upper surface it is bounded by a fluid flow (see figure 1). The derivation is performed for a compressible material; however results are given for the incompressible case only. The differential equation of motion for a Voigt material is (see Fung 1965)

$$\frac{\partial^2 \boldsymbol{\zeta}}{\partial t^2} = C_{\mathrm{T}}^2 \nabla^2 \boldsymbol{\zeta} + (C_{\mathrm{L}}^2 - C_{\mathrm{T}}^2)\, \boldsymbol{\nabla}(\boldsymbol{\nabla} \cdot \boldsymbol{\zeta}), \tag{1}$$

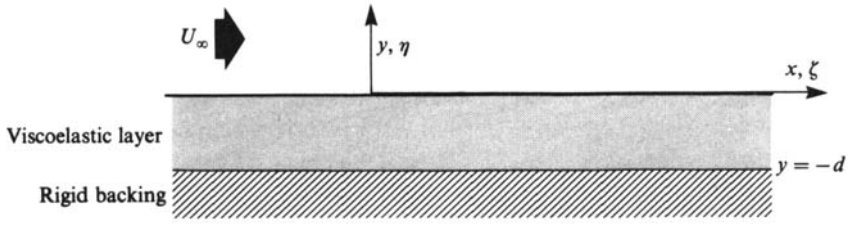

FIGURE 1. Schematic of the flow–coating system.

where $\boldsymbol{\zeta}$ is the displacement vector $(= \xi\hat{\imath} + \eta\hat{\jmath})$ and C_T and C_L are the shear and longitudinal wave speeds of the solid. In wave number–phase speed space for small strains they take the form

$$C_T^2 = C_t^2(1 - ikd\,C\gamma_t), \quad C_L^2 = C_\ell^2\left(1 - ikd\,C\frac{C_t}{C_\ell}\gamma_\ell\right), \tag{2}$$

where C_t^2 and C_ℓ^2 are the real parts of C_T^2 and C_L^2, k is the wavenumber $(2\pi/\lambda)$, $C(= c/C_t)$ is the dimensionless phase speed, and γ_t and γ_ℓ are the dimensionless damping ratios defined as

$$\gamma_t = \frac{\tau_t C_t}{d}, \quad \gamma_\ell = \frac{\tau_\ell C_\ell}{d}. \tag{3}$$

The relaxation times τ_t and τ_ℓ indicate the dissipative properties of the materials. For incompressible materials, the damping properties are sometimes reported in terms of the loss tangent, $\tan\delta$, rather than τ_t. In terms of the loss tangent $\tau_t = \tan\delta/\omega_r$, where ω_r is the frequency of the wave motion.

There are four boundary conditions for the present problem. In their linearized form they can be written:

$$\sigma_{yy} = -P_f - P_d, \quad y = 0, \tag{4}$$

$$\sigma_{xy} = 0, \quad y = 0, \tag{5}$$

$$\zeta = 0, \quad y = -d, \tag{6}$$

$$\eta = 0, \quad y = -d, \tag{7}$$

where σ_{yy} and σ_{xy} are the normal and shear stresses which have the form

$$\sigma_{yy} = 2\rho C_T^2\frac{\partial\eta}{\partial y} + \rho(C_L^2 - 2C_T^2)\left(\frac{\partial\zeta}{\partial x} + \frac{\partial\eta}{\partial y}\right), \tag{8}$$

$$\sigma_{xy} = \rho C_T^2\left(\frac{\partial\zeta}{\partial y} + \frac{\partial\eta}{\partial x}\right). \tag{9}$$

Boundary conditions (6) and (7) state that there is no horizontal or vertical displacement at the lower boundary, $y = -d$. The continuity of force conditions at the upper boundary are given by (4) and (5). In the present model the flow pressure and the vertical stress component in the coating are matched at the interface, while the shear stress is taken to be zero. This approximation and the forms for the pressures will be examined later.

For initial conditions it is assumed that there are no disturbances in the coating at $t = 0$. Thus

$$\zeta = \dot{\zeta} = 0, \quad t = 0, \quad \infty \leqslant x \leqslant \infty, \quad -d \leqslant y \leqslant 0. \tag{10}$$

2.2. *Transformation of the problem*

The solution of these equations is obtained by standard techniques which are outlined below. The reader is referred to Miklowitz (1978) for a more detailed account. Basically, the displacement field is broken into irrotational and incompressible parts and then Fourier transformed in x and Laplace transformed in time. The equations of motion lead to ordinary differential equations in y and these are solved analytically. In transform space the displacements are then

$$\left.\begin{aligned}\tilde{\bar{\xi}} &= \frac{ik}{\alpha}\sinh(\alpha y)\,A + ik\cosh(\alpha y)\,B + \cosh(\beta y)\,C + \beta\sinh(\beta y)\,D,\\ \tilde{\bar{\eta}} &= \cosh(\alpha y)\,A + \alpha\sinh(\alpha y)\,B - \frac{ik}{\beta}\sinh(\beta y)\,C - ik\cosh(\beta y)\,D,\end{aligned}\right\} \tag{11}$$

where

$$\alpha^2 = k^2\left(1+\frac{p^2}{k^2C_{\mathrm{L}}^2}\right), \quad \beta^2 = k^2\left(1+\frac{p^2}{k^2C_{\mathrm{T}}^2}\right), \tag{12}$$

and the Fourier and Laplace transforms of a variable Q are defined as

$$\left.\begin{aligned}\bar{Q}(k,y,t) &= \int_{-\infty}^{\infty} Q(x,y,t)\,\mathrm{e}^{-ikx}\,\mathrm{d}x,\\ \tilde{Q}(x,y,p) &= \int_{0}^{\infty} Q(x,y,t)\,\mathrm{e}^{-pt}\,\mathrm{d}t,\end{aligned}\right\} \tag{13}$$

where $p = -ikc$ and c is the complex phase speed. The four constants A, B, C and D in (11) will be evaluated through the four boundary conditions (4)–(7). However, the pressure terms P_{d} and P_{f} must be evaluated first.

2.3. *Forms for the surface pressure*

The disturbance pressure that drives the coating motion is given by P_{d}, while the induced pressure component P_{f} models the effect of the mean flow over the wavy surface. The disturbance-pressure term models the pressure footprint caused by an individual turbulent burst or eddy in the boundary layer. It is realized that the pressure disturbance is accompanied by a shear-stress variation that is significant but somewhat smaller in magnitude (Willmarth 1975). However, the effect of the shear stress is left to later studies. An approximate general form for the pressure is

$$P_{\mathrm{d}} = P_0\,g(t)\,f(x-U_{\mathrm{d}}\,t), \tag{14}$$

where U_{d} is the convection speed of the disturbance which is always less than U_∞. Equation (14) is used to model a pressure distribution of constant shape f that is convected at a constant speed, grows in strength from zero to a maximum and then decays back to zero according to the function g. The shape function f is chosen to approximate the pressure distribution from a vortex moving over a rigid surface at constant speed, strength and height a. Thus

$$f(x-U_{\mathrm{d}}\,t) = \frac{a^2}{a^2+(x-U_{\mathrm{d}}\,t)^2}. \tag{15}$$

The vortex height a is chosen as the distance from the wall where the mean flow velocity in the boundary layer equals the convection speed of the pulse. Measurements of pressure fluctuations on rigid walls (Willmarth 1975) have shown that most pressure distributions move at a speed of $0.8U_\infty$. For Reynolds numbers based on

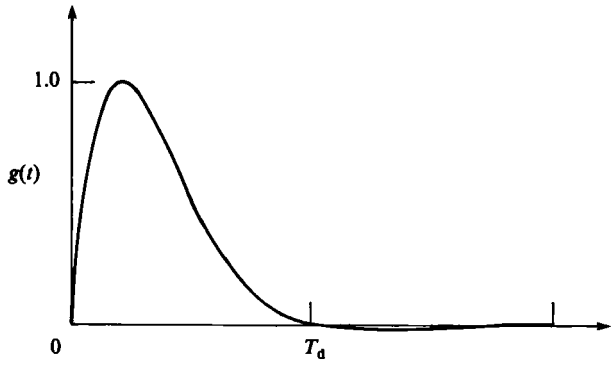

FIGURE 2. The temporal behaviour of the disturbance pressure: $g(t) = e^{-4t} \sin(\pi t)/0.26461$.

a downstream distance between 5.0×10^5 and 10^7, the $\frac{1}{7}$th-power law can be used. Thus $a = 1.7\delta^*$, where δ^* is the displacement thickness of the boundary layer. The strength P_0 can also be taken from Willmarth (1975)

$$P_0 = 0.0055 \rho_f U_\infty^2. \tag{16}$$

Finally a form for $g(t)$ must be chosen. Willmarth (1975) reports that the pressure events last for the time T_d, in which they travel about six of their own lengthscales (in this case $2a$). Thus the $g(t)$ must be zero for $t < 0$ and $t > T_d$ and must increase to a maximum and then decay in the interval $0 < t < T_d$. The following equation, which approximates this behaviour, was chosen for mathematical convenience:

$$g(t) = \frac{e^{rt} \sin(st)}{[e^{rt} \sin(st)]_{\max}}, \tag{17}$$

where $s = \pi/T_d = \pi U_d/12a$. The ratio r/s is set to $-4/\pi$, and this implies $[e^{rt} \sin(st)]_{\max} = 0.264\,16$. A plot of the function appears in figure 2. Using (15) and (17), the Fourier–Laplace transform of the disturbance pressure is

$$\tilde{\tilde{P}}_d = \frac{P_0 \pi s a \, e^{-a|k|}}{[e^{rt} \sin(st)]_{\max} [(p + ikU_d - r)^2 + s^2]}. \tag{18}$$

The induced pressure P_f is modelled with a modified potential flow as used by Duncan *et al.* (1985). In this model, the equation for the pressure due to a potential flow over the wavy surface is derived first. In transform space it has the form

$$\tilde{\tilde{P}}_f|_{\text{potential}} = -\rho_f k \left(U_\infty - \frac{ip}{k}\right)^2 \tilde{\tilde{\eta}}|_{y=0}. \tag{19}$$

Of course, any real boundary-layer flow does not follow this potential-flow result. In order to account for the boundary layer, the prediction of the potential flow is altered to include a reduced magnitude and a phase shift. Thus the pressure term takes the form

$$\tilde{\tilde{P}}_f = -K_f \rho_f k \left(U_\infty - \frac{ip}{k}\right)^2 e^{i\phi_f} \tilde{\tilde{\eta}}|_{y=0}. \tag{20}$$

This is a reasonable approximation in view of Kendall's (1970) experimental data and Benjamin's (1959) theoretical results.

2.4. *Solution in the transformed space*

In the transformed space the problem is solved by placing the solutions to the equations of motion (11) and the forms for the surface pressures, (18) and (20), into the boundary conditions (4)–(7) and solving for the constants in (11). In the present case, the vertical displacement at the surface of the coating is required. This is obtained from (11):

$$\tilde{\bar{\eta}}|_{y=0} = A - \mathrm{i}kD. \tag{21}$$

Thus, only the two constants A and D need to be evaluated. From linear algebra,

$$A = \frac{\mathrm{COF}_{11}}{\mathrm{DET}}, \quad D = \frac{\mathrm{COF}_{14}}{\mathrm{DET}}, \tag{22}$$

where

$$\mathrm{COF}_{11} = C_{\mathrm{T}}^2(k^2+\beta^2)\left(\frac{k^2}{\beta}\cosh(\alpha d)\sinh(\beta d) - \alpha\sinh(\alpha d)\cosh(\beta d)\right), \tag{23}$$

$$\mathrm{COF}_{14} = -2\mathrm{i}kC_{\mathrm{T}}^2\left(\frac{k^2}{\beta}\cosh(\alpha d)\sinh(\beta d) - \alpha\sinh(\alpha d)\cosh(\beta d)\right), \tag{24}$$

$$\begin{aligned}\mathrm{DET} = {} & \frac{\rho_{\mathrm{f}}}{\rho_{\mathrm{c}}}K_{\mathrm{f}}\left(\frac{U_\infty}{C_t}-C\right)^2 \mathrm{e}^{\mathrm{i}\theta_t}k(\beta^2-k^2)\left(\frac{k^2}{\beta}\cosh\alpha d\sinh\beta d - \alpha\cosh\beta d\sinh\alpha d\right) \\ & -4\frac{C_{\mathrm{T}}^2}{C_{\mathrm{t}}^2}(k^2+\beta^2)k^2 + \frac{C_{\mathrm{T}}^2}{C_{\mathrm{t}}^2}(k^2+\beta^2)^2\left(\cosh\alpha d\cosh\beta d - \frac{k^2}{\alpha\beta}\sinh\alpha d\sinh\beta d\right) \\ & +4\frac{C_{\mathrm{T}}^2}{C_{\mathrm{t}}^2}k^2(k^2\cosh\alpha d\cosh\beta d - \alpha\beta\sinh\alpha d\sinh\beta d).\end{aligned} \tag{25}$$

2.5. *Inversion of the transform*

The inversion of the Laplace transform for the displacement,

$$\bar{\eta}|_{y=0} = \frac{1}{2\pi\mathrm{i}}\int_{\gamma-\mathrm{i}\infty}^{\gamma+\mathrm{i}\infty}\tilde{\bar{\eta}}|_{y=0}\,\mathrm{e}^{pt}\,\mathrm{d}p, \tag{26}$$

is performed in a manner similar to Miklowitz (1978). The interested reader is referred to his book for a detailed account of the method. Briefly, a contour integration is carried out and it is shown that the integral in (26) is equal to the sum of the contributions from each of the poles of $\tilde{P}_{\mathrm{d}}$ and the places where DET = 0. Performing these operations and inverting the fourier transform we find that the displacement in physical space has the form

$$\begin{aligned}\eta_1|_{y=0} = {} & \frac{-P_0}{2\pi(0.26416)}\int_{-\infty}^{\infty}\left\{\sum_{p'=r+\mathrm{i}s,\,r-\mathrm{i}s}\left[\frac{\pi sa\,\mathrm{e}^{-a|k|}}{2(p'-r)}\frac{\mathrm{COF}_{11}-\mathrm{i}k\,\mathrm{COF}_{14}}{\mathrm{DET}}\mathrm{e}^{\mathrm{i}kx'+p't}\right]\right. \\ & \left. + \sum_{j=-\infty}^{\infty}\left[\frac{\pi sa\,\mathrm{e}^{-a|k|}}{(p'-r)^2+s^2}\frac{\mathrm{COF}_{11}-\mathrm{i}k\,\mathrm{COF}_{14}}{(\mathrm{d}\,\mathrm{DET}/\mathrm{d}p)}\mathrm{e}^{\mathrm{i}kx'+p't}\right]_{p=p_j}\mathrm{d}k\right\},\end{aligned} \tag{27}$$

where

$$p' = p + \mathrm{i}kU_{\mathrm{d}}, \quad x' = x - U_{\mathrm{d}}t.$$

The p, k (or equivalently c, k) pairs for which DET = 0 define the dispersion relation for elemental plane waves in the flow-coating system. Note that the effect of the flow on the dispersion relation enters through the induced-pressure term in (4). The zeros of the determinant were found numerically using a contour integration technique based on the work of Delves & Lyness (1967). The Fourier transform was also inverted numerically.

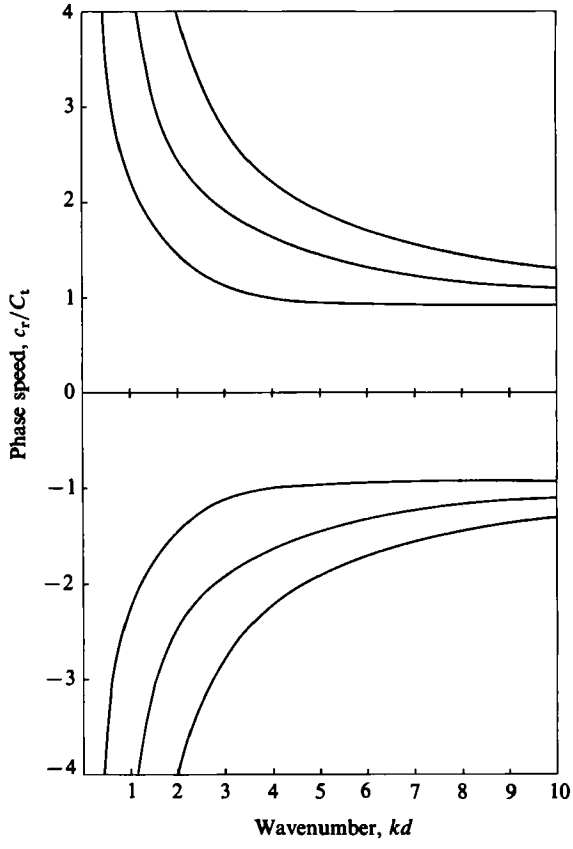

FIGURE 3. Dispersion curves – modes 1, 2 and 3: $U_\infty/C_t = 0$, $K_f = 0.25$, $\phi_f = 0$, $\rho_f/\rho_c = 1.0$, $C_\ell/C_t = 70.0$, $\gamma_t = 0$.

3. Results

3.1. *Dispersion curves and stability*

The propagation and stability of interfacial waves in the present flow-coating system was discussed in detail by Duncan *et al.* (1985). The examples used in their work were primarily cases with high damping. The essential details of their discussion will be briefly summarized below and the examples will be extended to a wide range of damping. In these examples, the density of the flow is equal to the coating density and the ratio C_ℓ/C_t is set to 70.0 (effectively incompressible). Using Kendall's (1970) data on flow over moving wavy walls, the pressure coefficient K_f is assumed as 0.25. The ratio of the wavelength to the boundary-layer displacement thickness in Kendall's experiment was about 17. Since, as will be seen later, the wavelengths in the present case are typically several times the coating thickness, the pressure coefficient from Kendall's work corresponds to a thick coating relative to the boundary-layer displacement thickness.

Plots of phase speed versus wavenumber for a purely elastic incompressible coating bounded by an ideal flow ($K_f = 0.25$, $\phi_f = 0$) are shown in figures 3 and 4 for flow speeds of 0 and $3.0C_t$ respectively. For zero flow speed (figure 3), the curves are symmetric about the $c = 0$ axis, indicating that waves propagate in the positive or

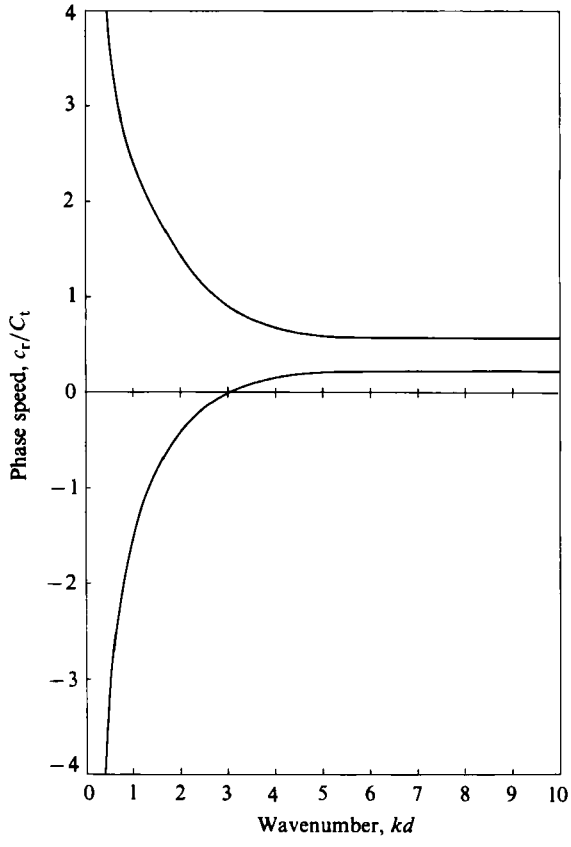

FIGURE 4. Dispersion curves – mode 1: $U_\infty/C_t = 3.0$, $K_f = 0.25$, $\phi_f = 0$, $\rho_f/\rho_c = 1.0$, $C_\ell/C_t = 70.0$, $\gamma_t = 0$.

negative x-direction with the same speed. Three sets of curves are shown representing three modes of wave propagation in the coating. The mode-1 curve is defined as the one with the lowest $|c|$. The phase-speed curves tend to infinity at small wavenumber and a constant value at large wavenumber. Of particular importance for the coating response is the existence of a minimum wave speed, which in this case is about $0.84C_t$. For a flow speed of $3.0C_t$ (figure 4), only the first mode is given since it is the most important for the coating response and the only one significantly effected by the flow. Note that the downstream (positive c) branch has changed little from the zero-flow-speed case. The upstream branch has moved toward the $c = 0$ axis, and for wavenumbers greater than about 3.0, the waves propagate downstream at slow speed. At still higher flow speeds, the upstream and downstream curves meet and a flutter instability appears.

The waves shown in figures 2 and 3 are neutrally stable in the ideal system with no damping in the coating and no phase shifts from the pressure distribution of a potential flow over the wavy surface. Damping causes an irreversible loss of mechanical energy from the coating. The pressure phase shift causes an irreversible transfer of energy between the flow and the interfacial waves system; the direction of the energy transfer depends on the wave direction and the sign of the pressure phase shift. When the flow speed is less than about C_t all waves in the system move

upstream or downstream at speeds greater than the flow speed. For all downstream-running waves with phase speed greater than the flow speed, the pressure phase is such that there is a force on the wave in the upstream direction (Sengupta & Lekoudis 1985), i.e. energy is transferred from the wave system to the flow. Thus for the downstream branch both the damping and the pressure phase shift cause energy to be removed from the wave. Duncan *et al.* (1985) have shown that at these low flow speeds all waves in the system are members of Benjamin's (1963) and Landahl's (1962) class B. This class of waves is stabilized by energy loss. Thus both the pressure phase shift and the damping tend to make the downstream-running waves decay for low flow speeds. For the upstream branch, the phase shift causes a force in the downstream direction; again both the damping and the phase shift remove energy from the wave system. These class-B waves decay also.

When the flow speed is above C_t, but less than the flutter speed, the downstream branch is still Class B, but some waves move slower than the flow. For these waves the pressure phase shift is in the downstream direction, and energy is transferred to the wave tending to make this class-B wave unstable. However, sufficient damping can be used to stabilize these waves. The rate of energy transfer from the flow increases as the difference between the wave speed and the flow speed increases. Thus, as the flow speed is increased, more damping will be required to stabilize the wave. As long as the flow speed is low, the upstream branch does not begin to propagate downstream; for these waves both the damping and the pressure phase shift will cause wave decay. Once the flow speed is increased to $U_\infty/C_t = 2.9$ the high-wavenumber portion of the upstream branch begins to propagate downstream (see figure 4); these are class-A waves. Class-A waves are stabilized by the pressure phase shift (which adds energy) and destabilized by the damping. Thus the damping that was added to stabilize the class-B waves from the downstream branch will destabilize the class-A waves from the upstream branch. Further increases in damping do not raise the onset flow speed for unstable waves.

Calculations to define the stability boundary as a function of damping were performed. K_f was again chosen as 0.25. When the damping is low the potentially unstable class-B waves move downstream at speeds in the range of C_t to $2C_t$, which turns out to be an appreciable fraction of the flow speed. For these waves a value of $-40°$ was chosen for ϕ_f. From Kendall's data, this value appears to be typical of waves moving at these speeds. At high damping the potentially unstable class-A waves move very slowly. Again, using Kendall's data, ϕ_f has been set to $-10°$ for these waves. The stability boundary determined with these pressure parameters appears as a dashed line in the plot of flow speed versus damping shown in figure 5. An error in choosing K_f and ϕ_f will change the results quantitatively somewhat but not qualitatively. The stability boundary at low damping is determined primarily by the minimum wave speed of the coating. Thus, regardless of the pressure coefficients the stability boundary will reach the lower limit shown in figure 5 ($U_\infty \approx C_t$) for sufficiently small damping. The stability limit at high damping occurs when the waves from the upstream dispersion curve begin to propagate downstream at high wavenumber. Duncan *et al.* have shown that this occurs at the flow speed given by

$$\left.\frac{U_\infty}{C_t}\right|_{\text{class A onset}} = \left(\frac{2}{K_f}\frac{\rho_c}{\rho_f}\right)^{\frac{1}{2}}. \tag{28}$$

The pressure coefficient K_f decreases with decreasing wavelength compared to boundary-layer thickness. As was pointed out earlier, the value used here is for relatively long waves, i.e. thick coatings. Thus, for thinner coatings, the onset speed

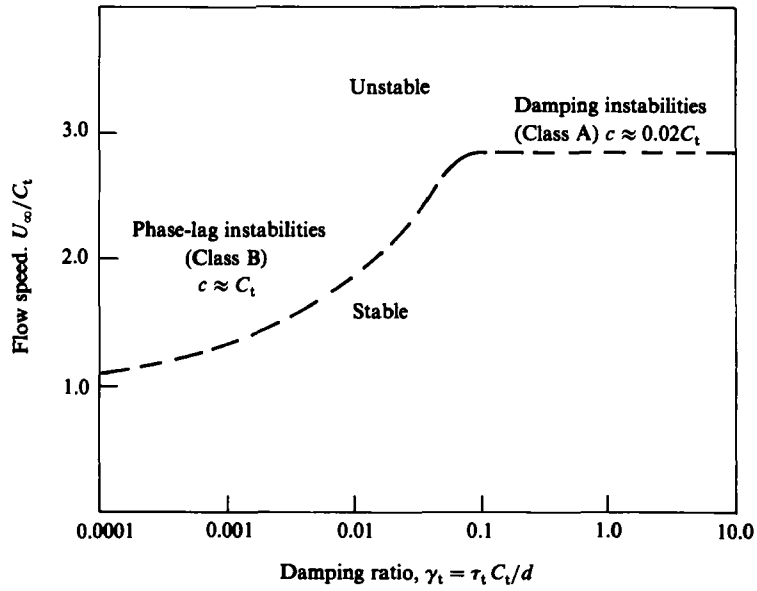

FIGURE 5. Regions of stable and unstable response on a plot of flow speed versus damping: $\rho_f/\rho_c = 1.0$, $K_f = 0.25$, $C_\ell/C_t = 70.0$.

at high damping will be increased. At the present time this effect cannot be properly quantified owing to insufficient theoretical and experimental data.

3.2. *Response calculations with* $\gamma_t = 0$

The response integral (27) was evaluated numerically using the dispersion curves discussed previously. The pulse characteristics were chosen as described in §2 to imitate the unsteady pressures on a rigid wall under a turbulent boundary layer. Thus, the pulse moves with $0.8U_\infty$, its shape is given by $a^2/(a^2+(x-U_d t)^2)$, the pulse half-width a is equal to $1.7\delta^*$, the pulse lasts for the time it takes to move $12a$, and it has a maximum strength of $0.0055\rho_f U_\infty^2$. With these restrictions the response is a function of three dimensionless variables: the flow speed (U_∞/C_t), the coating thickness (d/δ^*) and the damping ratio (γ_t). In the following, the response is first explored for a coating with no damping in the range of flow speeds from 0 to 2.8, even though the response would not be stable at the higher flow speeds in the presence of a real boundary layer. Then the effect of damping on the elastic results is examined in §3.5.

The influence of d/δ^* and U_∞/C_t on the coating response is illustrated in the six time sequences of vertical surface displacement versus horizontal position shown in figure 6. Each time sequence consists of five distributions of surface displacement at $t = 0.2T_d$, $0.4T_d$, $0.6T_d$, $0.8T_d$ and $1.0T_d$. Both the horizontal coordinate and the vertical displacement are normalized by the boundary-layer displacement thickness. The vertical scale in the left column is three times that in the right column. Note that the horizontal position is given in the reference frame of the pulse. In the left column of the figure (a, c, e), $U_\infty/C_t = 1.0$, while in the right hand column (b, d, f) $U_\infty/C_t = 2.5$. The coating thickness is $8.0\delta^*$ in the upper pair (a, b), $4.0\delta^*$ in the middle pair (c, d), and $0.8\delta^*$ in the bottom pair (e, f).

One of the most important results illustrated by figure 6 is that the response

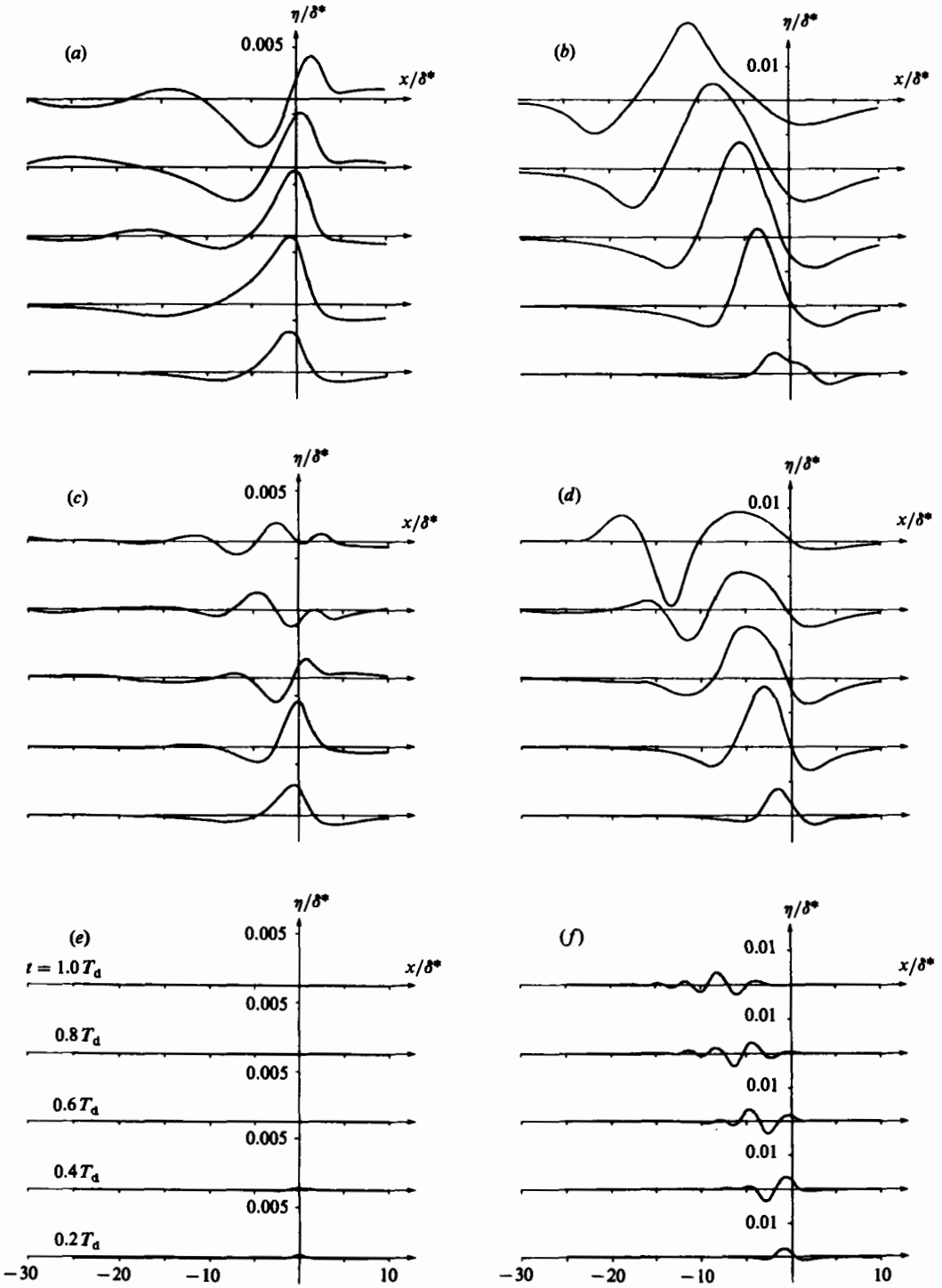

FIGURE 6. Six time histories of vertical displacement at the coating surface. Each time history contains five plots of displacement versus x at $t = 0.2T_d$, $0.4T_d$, $0.6T_d$, $0.8T_d$ and $1.0T_d$. All plots are in the reference frame of the pulse. $K_t = 0.25$, $\phi_t = 0$, $\rho_t/\rho_c = 1.0$, $C_\ell/C_t = 70.0$, $\gamma_t = 0$. (*a*) $U_\infty = C_t$, $d = 8.0\delta^*$; (*b*) $2.5C_t$, $8.0\delta^*$; (*c*) C_t, $4.0\delta^*$; (*d*) $2.5C_t$, $4.0\delta^*$; (*e*) C_t, $0.8\delta^*$; (*f*) $2.5C_t$, $0.8\delta^*$.

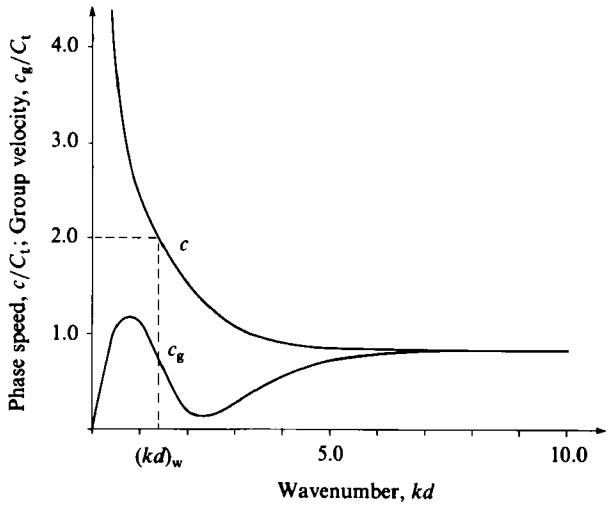

FIGURE 7. Phase speed and group velocity versus wavenumber – mode 1, downstream branch: $U_\infty/C_t = 2.5$, $K_f = 0.25$, $\phi_f = 0$, $\rho_f/\rho_c = 1.0$, $C_\ell/C_t = 70.0$, $\gamma_t = 0$.

consists mainly of waves behind the pulse for the higher-flow-speed cases, while for the lower-flow-speed cases the maximum response is local with smaller waves both ahead of and behind the pulse. The change from a local to a following-wave response occurs at $U_\infty/C_t = 1.2$ ($U_d = 0.96C_t$). A shift in the phase of the response just under the pulse ($-1.7\delta^* < x < 1.7\delta^*$) occurs at the same flow speed. For U_∞/C_t less than 1.2 the response is nearly symmetric (at least at early times), while for higher speeds it is shifted, with the peak just behind the pulse. The phase shift at the higher flow speed indicates a horizontal force on the coating. Note also that in the two cases with thinner coatings and high flow speed (d, f) the positions of the peaks and troughs of the following waves are fairly steady relative to the pulse. For the thickest coating, the pattern behind the pulse in the high-speed case consists of a single peak which continually moves backward from the pulse.

Many of the above observations can be explained using the dispersion curves. Consider first the change in the character of the response at $U_\infty/C_t = 1.2$. The total response of the coating consists of a local response, which is confined to the vicinity of the pulse, and a wavelike response, which can contribute at all positions. The local response arises from the singularities in the pressure transform $\tilde{P}_d$ (the first term in (27)). The wavelike response consists of the free waves excited by the pulse and is calculated from the second term in (27). The dominant part of the free-wave contribution to the response consists of waves whose phase speed equals the pulse speed, i.e. the positions of the crests and troughs are fairly steady relative to the pulse. A plot of phase speed versus wavenumber for $U_\infty/C_t = 2.5$ is shown in figure 7. The horizontal line is drawn at the pulse speed ($2.0C_t$). The intersection of this line and the phase-speed curve indicates the wave that moves with the pulse, i.e. the dominant free wave in the response. Note that all the dispersion curves show a minimum phase speed for the downstream-running waves. This minimum ranges between 0.74 and 0.96 depending on the flow speed. For flow speeds below 1.2, it turns out that the pulse speed ($0.8U_\infty$) is always less than the minimum wave speed and there can be no waves moving with the pulse. Thus the contribution from the free waves is smaller and the dominant part of the response is local to the pulse. The

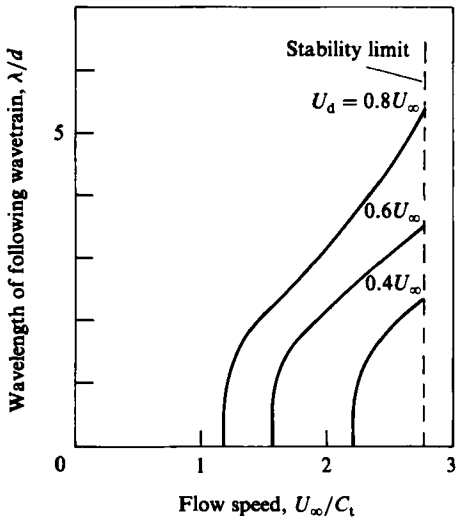

FIGURE 8. Wavelength of following wavetrain versus flow speed for various values of U_d/U_∞: $K_f = 0.25$, $\phi_f = 0$, $\rho_f/\rho_c = 1.0$, $C_f/C_t = 70.0$, $\gamma_t = 0$.

additional energy needed to generate the following wavetrain at the higher flow speeds is obtained through the horizontal force on the asymmetric surface shape under the pressure pulse. Thus it appears that this force is a wave drag.

In the high-speed cases, the position of the following waves relative to the pulse is determined by the group velocity of the dominant wave compared to its phase velocity. If the group velocity is less than the phase velocity the waves are left behind, while for group velocities greater than the phase velocity the waves are ahead of the pulse. A plot of the group velocity for the first-mode downstream dispersion curve is included in figure 7. Note that the group velocity is everywhere less than the phase velocity, showing that the waves should be behind the pulse.

The phase-speed and group-velocity curves can be used to compute the wavelength and the number of waves in the following wavetrain. The wavelength is just $2\pi/(kd)_w$ where $(kd)_w$ is the wavenumber at the intersection of the phase-speed and the pulse-speed curves as shown in figure 7. A plot of the wavelength of the following wavetrain versus flow speed is shown in figure 8. Since in real boundary-layer flows pressure pulses move with speeds from $0.4U_\infty$ to $0.8U_\infty$, curves for U_d equal to $0.8U_\infty$, $0.6U_\infty$ and $0.4U_\infty$ are presented. Note that the wavelength is proportional to d and that the factor of proportionality increases with flow speed on each curve. The curves start at the respective onset speed of the following wavetrain for each pulse speed and end at the flow-speed stability limit ($U_\infty = 2.8C_t$).

To determine the maximum number of waves in the pattern the group velocity is needed. The pattern increases in length at a rate

$$\dot{X} = [c - c_g]_{k=k_w} \tag{29}$$

during the lifetime of the pulse. Thus, the total number of waves generated is

$$n = \frac{T_d \dot{X}}{\lambda} = 20.4 \frac{kd}{2\pi} \left(\frac{c - c_g}{C_t}\right) \frac{C_t}{U_d} \frac{\delta^*}{d}\bigg|_{k=k_w}. \tag{30}$$

The results are plotted in figure 9. Curves are shown for $U_d = 0.8U_\infty$, $0.6U_\infty$ and $0.4U_\infty$. From pressure measurements on rigid walls (Willmarth 1975), it appears

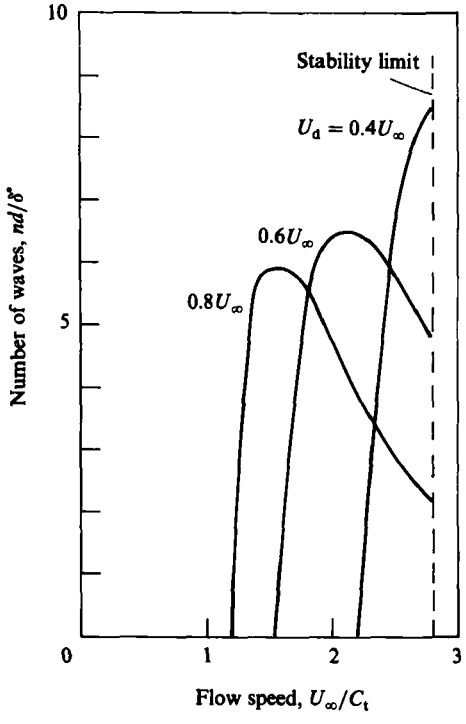

FIGURE 9. Number of waves in the following wavetrain versus flow speed: $K_f = 0.25$, $\phi_f = 0$, $\rho_t/\rho_c = 1.0$, $C_\ell/C_t = 70.0$, $\gamma_t = 0$.

that some of the slower pressure pulses last for considerably longer than the six lengthscales of travel used in the above calculations. In these cases the results in figure 9 can be scaled linearly.

In the high-flow-speed case with the thickest coating, figure 6(*b*), the single following wave is not steady relative to the pulse. There are two reasons for this result. First, (30) shows that the number of waves is proportional to δ^*/d. Thus as the coating thickness is increased the number of waves decreases. Using figure 9, with the conditions corresponding to figure 6(*b*), we find the number of waves generated to be 0.36, i.e. a steady wavetrain does not have time to form during the life of the pulse. Secondly, as the coating becomes thick it begins to behave like a semi-infinite solid. Surface waves on a semi-infinite solid are dispersionless, having only one wave speed (the minimum wave speed of the first-mode dispersion curves shown here). For pulse speeds greater than the wave speed, these waves are left behind in the form of a single peak as shown in figure 6(*b*). When the pulse moves slower than the minimum wave speed, as in figure 6(*a*), the waves begin to move ahead of the pulse.

The amplitude of the response is a particularly important parameter for evaluating the possibility of a significant interaction between a turbulent flow structure and the coating. Note from figure 6 that the amplitude of the response grows as the coating thickness increases. This is partly because the coating is incompressible. When the pulse width is much larger than the coating thickness, figures 6(*e*, *f*), the coating is hard to deform since it cannot be compressed, and material would have to be moved horizontally to deform the surface vertically. As the coating thickness increases, the deformations are easier to make, and the amplitude grows. The effect of flow speed

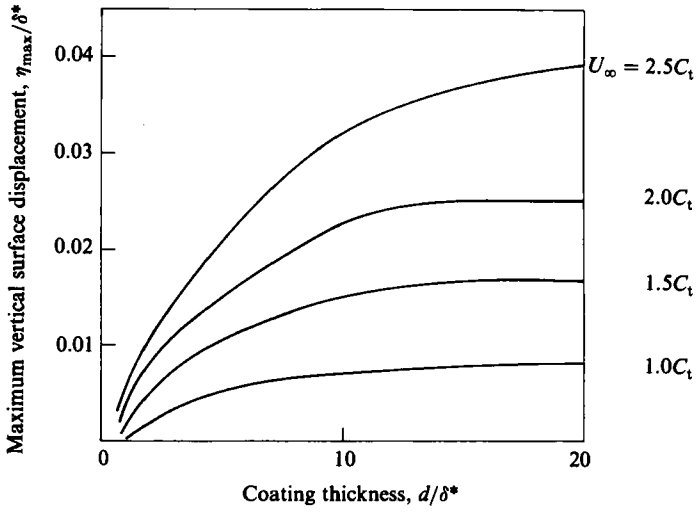

FIGURE 10. Maximum vertical surface displacement versus coating thickness for various speeds: $K_f = 0.25$, $\phi_f = 0$, $\rho_f/\rho_c = 1.0$, $C_\ell/C_t = 70.0$, $\gamma_t = 0$.

and coating thickness on maximum response amplitude is summarized in a plot of maximum vertical displacement versus coating thickness, figure 10. Separate curves are shown for flow speeds of $1.0C_t$, $1.5C_t$, $2.0C_t$ and $2.5C_t$. The displacements and the coating thickness are non-dimensionalized by δ^*. Note that maximum displacement increases smoothly with coating thickness for each flow speed, asymptoting to a constant value when the coating becomes effectively infinite, $d/\delta^* > 18$. The maximum displacement also increases with flow speed and reaches a maximum of about 4% δ^* at $U_\infty/C_t = 2.5$ and $d/\delta^* > 18$.

Also of interest is the horizontal position of the maximum displacement X_m relative to the pulse position. Figure 11 contains a plot of X_m/δ^* versus d/δ^* with four separate curves for the flow speeds used in figure 10. The maximum surface displacement always occurs behind the pulse centreline. The position of the maximum displacement increases with flow speed and coating thickness. The figure demonstrates that the largest vertical displacements in figure 10 occur outside the pulse half-width, $1.7\delta^*$.

3.3. *Energy transfer*

The energy transferred from the pressure pulse to the coating–mean flow system is an important quantity for assessing the possibility of influencing the behaviour of a turbulent flow structure. In this section calculations are presented which show the energy transfer as a function of U_∞/C_t and d/δ^*. The total energy transferred during the lifetime of the pulse is given by

$$E_t = \int_0^\infty \int_{-\infty}^\infty P_d \left.\frac{\partial \eta}{\partial t}\right|_{y=0} \mathrm{d}x\,\mathrm{d}t. \tag{31}$$

The expression for η given in §3.2 may be used to evaluate the total energy transfer. Thus, after some algebraic manipulation (31) becomes

$$E_t = \frac{1}{(2\pi)^2 \mathrm{i}} \int_{-\infty}^\infty \int_{\gamma-\mathrm{i}\infty}^{\gamma+\mathrm{i}\infty} p \tilde{\tilde{P}}_d(p', k)\, \tilde{\tilde{P}}_d(-p', k) \frac{\mathrm{COF}_{11} - \mathrm{i}k\mathrm{COF}_{14}}{\mathrm{DET}} \mathrm{d}k\,\mathrm{d}p', \tag{32}$$

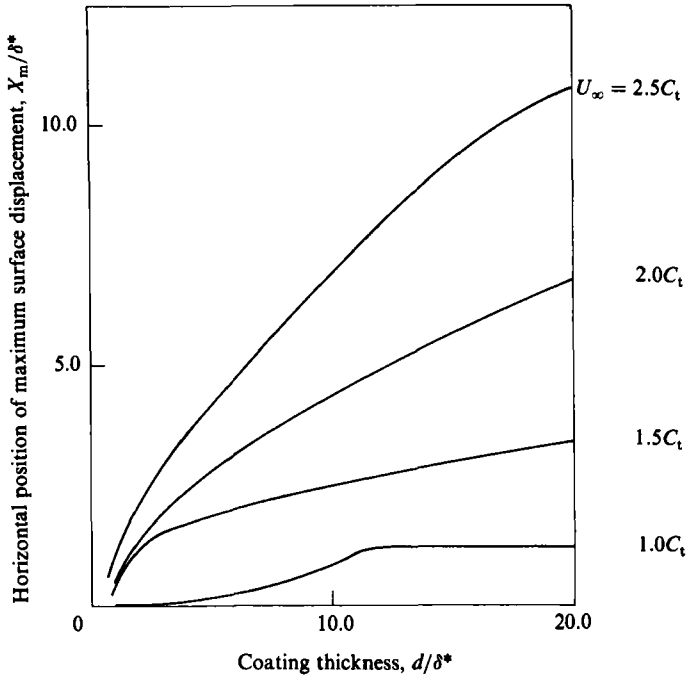

FIGURE 11. Horizontal position of maximum surface displacement versus coating thickness for various flow speeds: $K_f = 0.25$, $\phi_f = 0$, $\rho_t/\rho_c = 1.0$, $C_\ell/C_t = 70.0$, $\gamma_t = 0$.

where $$p' = p + ikU_d.$$

As in evaluating the expression for the displacement, the Laplace transform is inverted first. It is found that, for elastic coatings, the contributions from the singularities in $\tilde{\tilde{P}}_d$ cancel out and the total energy transfer becomes

$$E_t = \frac{1}{2\pi}\int_{-\infty}^{\infty}\left[p\tilde{\tilde{P}}_d(p', k)\,\tilde{\tilde{P}}(-p', k)\frac{\mathrm{COF}_{11} - ik\mathrm{COF}_{14}}{(\mathrm{d\,DET}/\mathrm{d}p)}\right]_{p=p_j}\mathrm{d}k. \tag{33}$$

Equation (33) was evaluated numerically for a variety of conditions and the results appear in a plot of energy transfer versus U_∞/C_t with curves of constant d/δ^* (figure 12). The energy is non-dimensionalized by $\delta^{*2}U_\infty^2$, the energy dissipated in a boundary layer during the lifetime of the pulse T_d over the distance travelled by the pressure pulse, $6(3.4\delta^*)$:

$$E_d = \tfrac{1}{2}\rho U_\infty^3\, C_f\, T_d(20.4\delta^*) \approx \delta^{*2}U_\infty^2 \quad \text{at } R_x = 5\times 10^5. \tag{34}$$

Note that each curve of constant d/δ^* in figure 12 starts with a very small value (less than 10^{-6}) at low flow speed. The energy transfer increases with flow speed for all coating thicknesses. For the thickest coating, a rapid increase of roughly two orders of magnitude occurs at around $U_\infty/C_t = 1.2$ – the speed where the surface deformations change from a local response to following-wave response (see §3.2). This is probably associated with the wave drag in the higher-flow-speed regime. Similar increases occur for the thinner coatings, but the increase is smaller and is delayed to higher flow speeds. Even at its maximum energy, the transfer is small compared to the dissipation scale, reaching only 5×10^{-4} for a flow speed of $2.0C_t$ and the thickest coating.

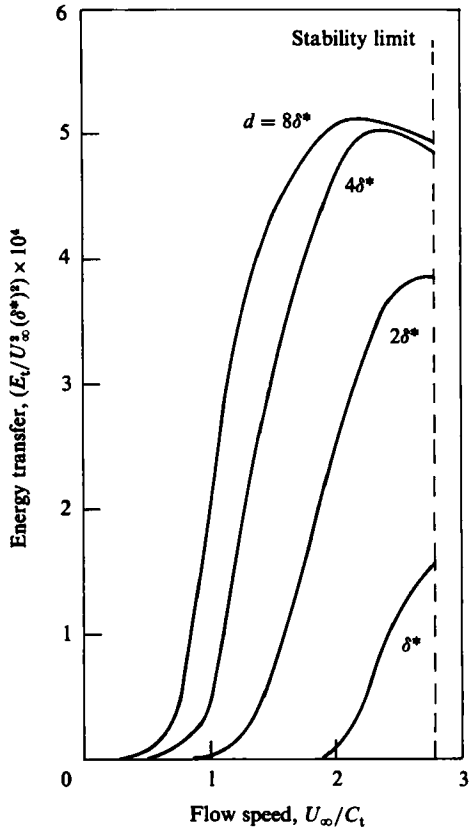

FIGURE 12. Energy transfer from the pressure pulse to the flow–coating system versus flow speed for various coating thicknesses: $K_t = 0.25$, $\phi_t = 0$, $\rho_t/\rho_c = 1.0$, $C_\ell/C_t = 70.0$, $\gamma_t = 0$.

3.4. *Wave patterns*

The dispersion relations from the two-dimensional theory can be used in an approximate, quasi-steady theory to obtain the lines of constant phase of the surface wave pattern for the full three-dimensional case. In this theory, the wave pattern is assumed to be much like the pattern from a steady source moving at constant speed, but the number of waves in the pattern is limited owing to the finite lifetime of the pulse. This assumption is validated by the results in figure 9, which predict that the pulse generates a number of waves in its lifetime.

Wave patterns produced by steady sources moving through dispersive media have been studied by a number of authors. In the present analysis, the results of Keller & Munk (1970) are used. The case of a wave source moving at constant strength and speed on a coating with no flow is examined first. It is then shown that the pattern in the presence of the flow is quite similar. In the zero-flow-speed case the wave propagation is horizontally isotropic and the relations describing the lines of constant phase are greatly simplified. From Keller & Munk

$$x + U_d t = \phi \frac{U_d(1 - cc_g/U_d^2)}{k(c - c_g)}, \quad z = \phi \frac{c_g(1 - c^2/U_d^2)^{\frac{1}{2}}}{k(c - c_g)}, \tag{35}$$

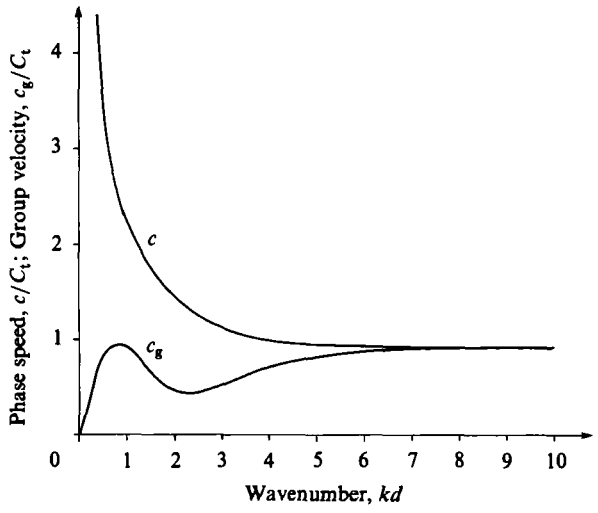

FIGURE 13. Phase speed and group velocity versus wavenumber – mode 1 downstream branch: $U_\infty/C_t = 0$, $K_f = 0.25$, $\phi_f = 0$, $\rho_f/\rho_c = 1.0$, $C_\ell/C_t = 70.0$, $\gamma_t = 0$.

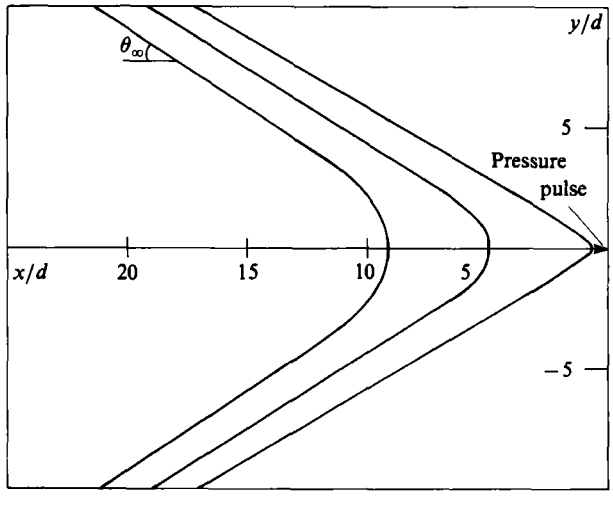

FIGURE 14. Three lines of constant phase for a steady pressure pulse: $U_d = 1.84C_t$, $U_\infty/C_t = 0$, $K_f = 0.25$, $\phi_f = 0$, $\rho_f/\rho_c = 1.0$, $C_\ell/C_t = 70.0$, $\gamma_t = 0$.

where ϕ is the phase and U_d is the speed of the pulse. These equations give the position of lines of constant phase as parametric functions of k, the wavenumber. Note that k appears both directly and indirectly through $c(k)$ and $c_g(k)$. Figure 13 contains a plot of c and c_g versus k for the zero-flow-speed case. Note that, as in the results for $U_\infty = 2.5C_t$ (figure 7), the waves become dispersionless ($c = c_g$) as $k \to \infty$ and that for all finite k, c_g is less than c. A plot of several lines of constant ϕ (= 1.0, 7.28, 13.56) obtained with the dispersion relations in figure 13 and a pulse speed of $U_d = 1.84C_t$ is shown in figure 14. The entire pattern is made of waves with $c \leqslant U_d$, a statement which is explained physically by the theory of Keller & Munk (1970) and verified by the necessity of keeping the radical in (35) real. For waves along the centreline, where the crests are normal to the direction of travel, the phase speed

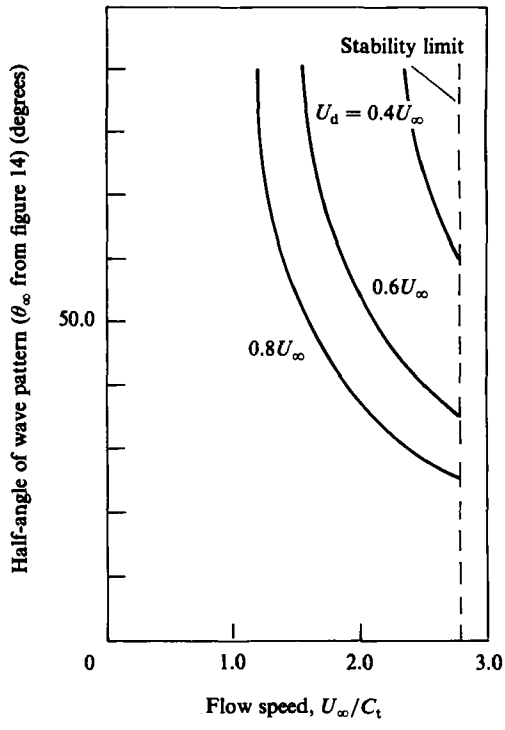

FIGURE 15. Half-angle (θ_∞) of the wave pattern due to a pressure pulse versus flow speed: $K_f = 0.25$, $\phi_f = 0$, $\rho_f/\rho_c = 1.0$, $C_\ell/C_t = 70.0$, $\gamma_t = 0$.

equals the pulse speed; the waves off the axis of travel have slower speeds and, consequently, shorter wavelengths (larger kd). The waves at the outskirts of the pattern ($kd \to \infty$) are dispersionless and (35) reduce to the equation of a straight line. The angle of these wavefronts to the direction of travel (see figure 14) is given by

$$\theta_\infty = \sin^{-1} \frac{c_\infty}{U_d}, \tag{36}$$

where c_∞ is the phase speed at large wavenumbers. Thus as the speed of the pulse is increased the angle of the pattern will decrease. The centreline wavelength increases with speed. Since the pattern is made of waves with $c \leqslant U_d$, there is no pattern if the pulse speed is less than the minimum wave speed.

In the case where a flow accompanies the moving pulse, the wave propagation is horizontally anisotropic because the flow speed in (25) must be replaced by the effective flow speed ($U_\infty \sin\theta$, where θ is the angle between the wave crest and the flow direction). Because the phase and group velocity curves for the downstream branches are qualitatively similar at all flow speeds (compare figures 7 and 13), one can expect that the wave patterns will also be similar to the zero-flow-speed case. In the centre section of the pattern, the lines of constant phase are nearly perpendicular to the flow direction, indicating $U_\infty \sin\theta = U_\infty$. Here the two-dimensional theory applies and the centreline wavelength (figure 8) and the number of waves (figure 9) were computed previously. Further from the pattern centreline, the lines of constant phase quickly become straight. The angle of these waves to the flow is still given by (36) where c_∞ is the wave speed at large k with the appropriate

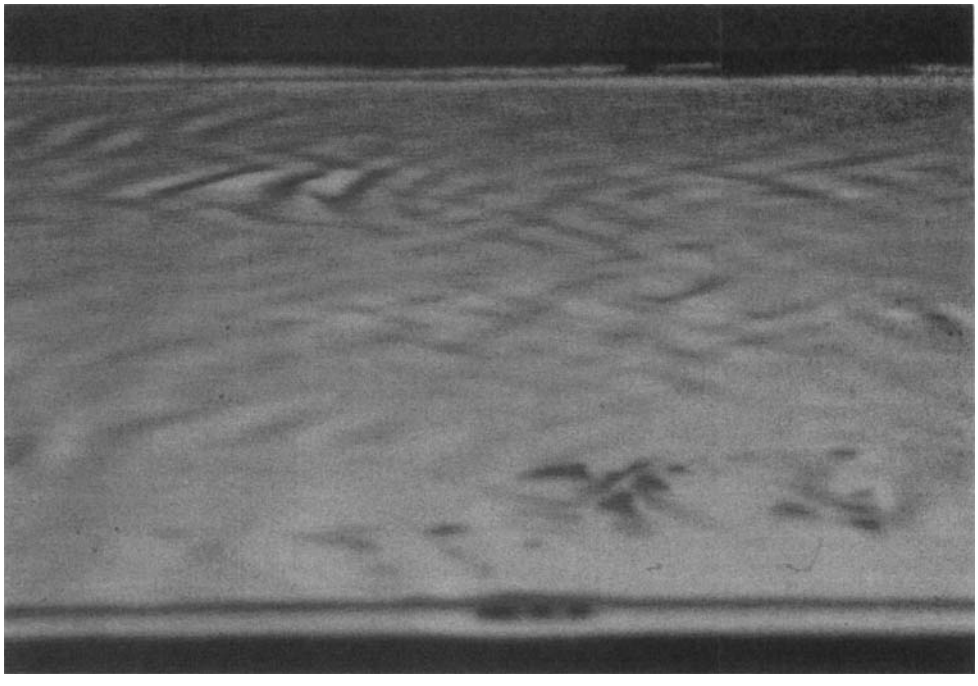

FIGURE 16. Wave patterns on a gelatin coating under a turbulent boundary layer. The flow is from right to left. The camera is looking down on the surface with a shallow angle (from the film by Chu, Falco & Wiggert 1984).

effective flow speed $U_\infty \sin\theta_\infty$. Since θ_∞ is not known, c_∞ is also undetermined. However, over the entire range of flow speeds c_∞ ranges from 0.96 to 0.74. The minimum value of 0.74 occurs at $U_\infty \sin\theta = 2.8$, the stability limit. The maximum value, 0.96, occurs at around $U_\infty \sin\theta = 1.0$. The range of effective flow speeds experienced by the waves in the outer parts of the pattern is considerably less. For instance, with $U_d = 0.8U_\infty$, the minimum flow speed to have a wave pattern is about $1.2C_t$. At this speed the outer parts of the pattern move in the flow direction ($\theta_\infty = 0$) and the effective flow speed is about $1.2C_t$. At the maximum flow speed ($U_\infty = 2.8$, $U_d = 2.24$) we find $\theta_\infty = 24°$, using a typical c_∞ of 0.9 in (36). This results in an effective flow speed of 1.13. Therefore, the effective flow speed for the outer parts of the pattern is always around 1.0 and we use $c_\infty = 0.96$ accordingly. Figure 15 contains a plot of θ_∞ versus flow speed for $U_d = 0.4U_\infty$, $0.6U_\infty$ and $0.8U_\infty$. Each curve begins at its own onset flow speed ($U_d = c_\infty$) and ends at the maximum stability limit for a coating with damping, $U_\infty = 2.8C_t$. The pattern angle decreases from 90° at onset to as low as 25° at the stability limit. For a given flow speed, the pattern angle increases as the pulse speed decreases. Chu, Falco & Wiggert (1984) have filmed the response of a Gelatin coating under a turbulent boundary layer. The data from the films has not been published as yet. Figure 16 is a still picture from their film showing a perspective view of several isolated wave patterns which look qualitatively similar to the pattern in figure 15. The flow direction is from right to left with magnitude $1.65C_t$.

3.5. *Response with damping*

The response calculations presented in the previous sections were performed with no material damping, $\gamma_t = 0$, and no pressure phase shift from the potential-flow calculation of the pressure distribution over the wavy surface. In §3.1 it was pointed out that for flow speeds above $1.0C_t$, pressure phase shifts in the mean boundary-layer flow over the wavy surface tend to destabilize the response. If damping is added to the material the stable range of flow speeds can be increased to $2.86C_t$ (see figure 5). In the ideal system used for the calculations of the previous sections, the response was neutrally stable. In the present section, several calculations are discussed which show the effect of the damping that must be added to stabilize the response in the presence of a real boundary layer.

Four sets of coating-response histories are shown in figures 17 (*a–d*). Each plot is for the same flow speed ($2.5C_t$) and coating thickness ($4\delta^*$). The damping ratio increases from 0.0 in figure 17 (*a*) to 1.0 in 17 (*d*). Figure 17 (*a*) is identical with figure 6 (*d*). The response shown in figure 17 (*b*) ($\gamma_t = 0.05$) is quite similar to the response with no damping; however the maximum amplitude is reduced by about 14 %. From the stability diagram in figure 5, it can be seen that this amount of damping is sufficient to stabilize the system up to a flow speed of about $2.7C_t$, very close to the maximum stable flow speed for any amount of damping. Thus, it appears that the response results of the previous sections in which the damping was set to zero are valid for the cases with sufficient damping to stabilize the response with a real boundary-layer flow.

The response with $\gamma_t = 0.3$ is shown in figure 17 (*c*). Here the maximum amplitude is reduced by 59 % from the response with $\gamma_t = 0$. Also note that the later parts of the following wavetrain have been almost completely damped out. The response in figure 17 (*d*), $\gamma_t = 1.0$, shows a viscous rather than a damped elastic character. The surface under the path of the pressure pulse is lifted by the low pressure and then relaxes back according to the relaxation time of the material τ_t. From the definition of γ_t, $\tau_t = d/C_t$ for this case. The time for the pulse to move over one of its own lengthscales is $3.4\delta^*/(0.8U_\infty)$ which is equal to $0.425d/C_t$ for $d = 4.0\delta^*$ and $U_\infty = 2.5C_t$. Thus the viscous relaxation time is larger than the timescale for the movement of the pulse. The length of the scar in figure 17 (*d*) covers nearly the entire distance travelled by the pulse ($20.4\delta^*$) in its lifetime. A response of this type (streamwise scars) was noted by Hansen *et al.* (1979) for turbulent flow over a plastisol coating. Panico & Kubota (1983) derived a similar result for a point load moving over a coating with no fluid flow. For γ_t above 1.0, the stiffness of the material begins to scale with the viscous properties of the material. The pressure available to deform the surface is proportional to U_∞^2. Its maximum value is limited by the stability limit on U_∞ ($2.8C_t$) which scales with the elastic properties of the material, even for large damping. Thus the amplitude of the response will continue to decrease as the damping is increased.

4. Overview

The characteristics of the response of an incompressible, viscoelastic coating are summarized on the plot of flow speed (U_∞/C_t) versus damping ratio ($\gamma_t = \tau_t C_t/d$) shown in figure 18. The dashed line divides the plot into an upper region where the response is unstable and a lower region where the response is stable. For low to moderate damping ($0 < \gamma_t < 0.05$), a phase-lag instability (Benjamin's class B)

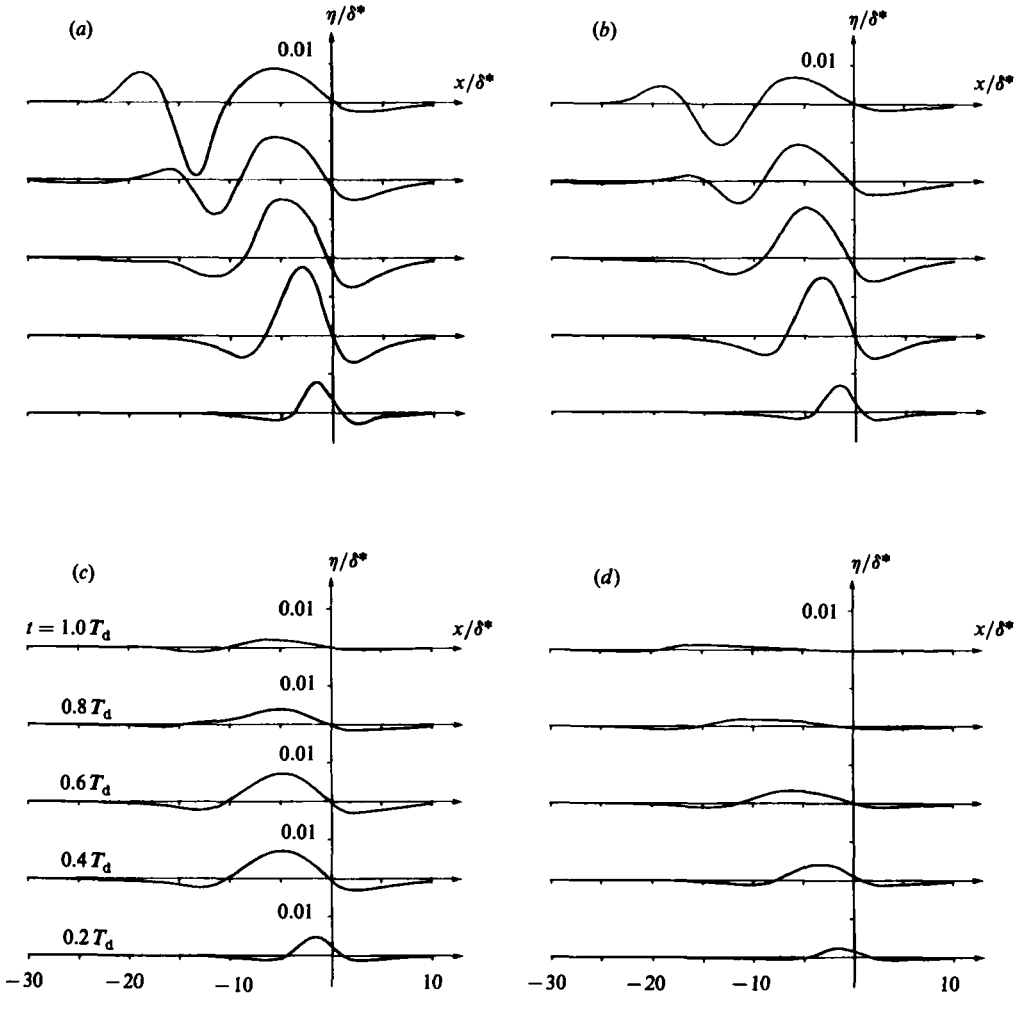

FIGURE 17. The effect of damping (γ_t) on the time history of the vertical displacement at the coating surface. Each time history contains five plots of displacement versus x at $t = 0.2T_d$, $0.4T_d$, $0.6T_d$, $0.8T_d$ and $1.0T_d$. All plots are in the reference frame of the pulse: $U_\infty/C_t = 2.5$, $U_d/C_t = 2.0$, $d/\delta^* = 4.0$, $K_f = 0.25$, $\phi_f = 0$, $\rho_f/\rho_c = 1.0$, $C_\ell/C_t = 70.0$. (*a*) $\gamma_t = 0$; (*b*) 0.05; (*c*) 0.3; (*d*) 1.0.

occurs first as the flow speed is increased. The onset flow speed for this instability increases from $1.0C_t$ at zero damping to nearly 2.8 at $\gamma_t = 0.05$. For $\gamma_t > 0.05$, a damping instability (Benjamin's class A) occurs at the stability boundary with an onset speed of $2.86C_t$. In the unstable region, the surface of the coating is covered with two-dimensional, organized wavetrains whose amplitude will be determined by nonlinear effects not considered in this paper. The response to turbulent flow events like bursts is of much smaller amplitude and is masked by the unstable waves. The region of stable response is divided into three subregions. For $\gamma_t < 0.5$ and flow speeds less than $1.2C_t$, the pressure pulses from the turbulent boundary layer move slower than the slowest interfacial wave of the flow–coating system. In this region, the response is symmetric to the pressure pulse for early times in the life of the pulse and at later times disturbances can move ahead of the pulse. The amplitude of the response increases with both flow speed and coating thickness and decreases slowly

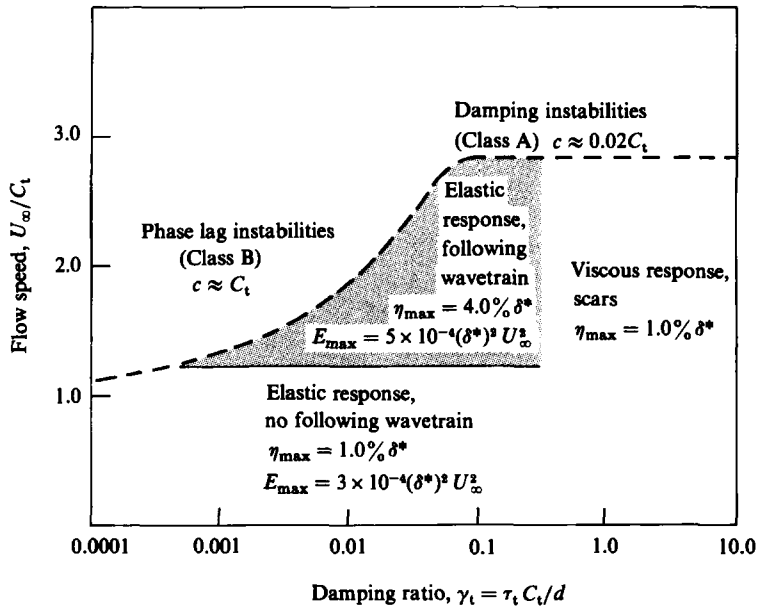

FIGURE 18. Summary plot: the response of an incompressible viscoelastic coating: $\rho_t/\rho_c = 1.0$, $K_t = 0.25$, $C_\ell/C_t = 70.0$.

with damping. The maximum amplitude η_{max} is about $0.01\delta^*$. When the flow speed is above $1.2C_t$ but less than the stability limit, and the damping ratio is less than 0.5, there are waves in the system with speeds less than or equal to the pulse speed. These waves form a V-shaped pattern behind the pulse. For a given ratio of pulse speed to flow speed, the centreline wavelength increases and the half-angle of the pattern decreases as the flow speed increases. The surface response just under the pressure pulse is antisymmetric, indicating a wave drag on the pulse. In this region, the response amplitude also increases with flow speed and coating thickness, reaching a maximum of $0.04\delta^*$ for $d > 18\delta^*$, flow speeds of $2.8C_t$, and $\gamma_t = 0.05$. This maximum amplitude, which is about equal to the viscous sublayer thickness at $R_x = 5 \times 10^5$, indicates the possibility of an interaction between the coating and the turbulent flow structures. It should be noted that the limit on response amplitude is a consequence of the limit on stable flow speeds. The coating deformations scale with the magnitude of the pressure fluctuations ($0.0055\rho U_\infty^2$) divided by the stiffness of the coating ($\rho_c C_t^2$). Since the flow becomes unstable with U_∞ exceeds $2.86C_t$, this ratio can not exceed 0.045 and the amplitudes are consequently limited.

The work done by the pressure pulse (the energy transferred from the pulse to the coating–mean flow system) increases slowly with flow speed at first, then, near $U_\infty = 1.2C_t$, it increases rapidly only to reach a new plateau for higher flow speeds. The work done increases with coating thickness. Its maximum value is $5.0 \times 10^{-4}\delta^{*2}U_\infty^2$ is about equal to the energy dissipated in the boundary layer over a length equal to the distance travelled by the pulse and over a time equal to the lifetime of the pulse.

In the high-damping region ($\gamma_t > 0.5$) the response is more viscous than elastic in character. The relaxation time of the material becomes greater than the pulse timescales and the response consists of a scar on the coating surface covering the

length travelled by the pressure pulse. The amplitude of the response decreases rapidly with increasing damping. Its maximum value is about $0.01\delta^*$ at $\gamma_t = 1.0$, $U_\infty = 2.8C_t$ and $d > 18\delta^*$.

5. Concluding remarks

The response of an incompressible, viscoelastic coating to pressure fluctuations in a turbulent boundary layer has been studied with a quasi-interactive model. The results indicate that the stable response of the coating may be large enough, at least at flow speeds near the stability limit, to alter the behaviour of turbulent flow structures in the boundary layer. The theory provides a guide for experiments or numerical investigations into the full interaction.

The support of the Office of Naval Research in the Compliant Coatings Drag Reduction program under contract N00014-81-0454 is gratefully acknowledged. The project was initiated by M. P. Tulin while the author was at Hydronautics, Incorporated. The author also wishes to acknowledge M. Cooper for numerous helpful discussions during the course of the work, and C. C. Chu, R. E. Falco and D. C. Wiggert for supplying the photograph in figure 16. Some aspects of this paper were presented at the Tenth Biennial Conference on Mechanical Vibration and Noise, ASME, Cincinnati, Ohio, September 1985, and the Winter Annual Meeting of the ASME, Miami, Florida, November 1985.

REFERENCES

BENJAMIN, T. B. 1959 Shearing flow over a wavy boundary. *J. Fluid Mech.* **6**, 161–205.

BENJAMIN, T. B. 1963 The threefold classification of unstable disturbances in flexible surfaces bounding inviscid flows. *J. Fluid Mech.* **16**, 436–450.

BUSHNELL, D. M., HEFNER, J. N. & ASH, R. L. 1976 Effect of compliant wall motion on turbulent boundary layers. *Phys. Fluids* **20**, S31–S48.

CHU, C. C., FALCO, R. E. & WIGGERT, D. C. 1984 Experimental determination of drag modification due to an elastic compliant surface using quantitative visual techniques. *Ninth Symp. on Turbulence, University of Missouri, Rolla*, pp. 42–1 to 42–7.

DELVES, L. M. & LYNESS, J. N. 1967 A numerical method for locating the zeros of an analytic function. *Maths Comp.* **21**, 543–560.

DOWELL, E. H. 1975 *Aeroelasticity of Plates and Shells.* Noordhoff.

DUNCAN, J. H., WAXMAN, A. M. & TULIN, M. P. 1985 The dynamics of waves at the interface between a viscoelastic coating and a fluid flow. *J. Fluid Mech.* **158**, 177–197.

FUNG, Y. C. 1965 *Foundations of Solid Mechanics.* Prentice-Hall.

GAD-EL-HAK, M. 1986*a* The response of elastic and viscoelastic surfaces to a turbulent boundary layer. *Trans. ASME* E: *J. Appl. Mech.* **53**, 206–212.

GAD-EL-HAK, M. 1986*b* Boundary layer interactions with compliant coatings: an overview. *Appl. Mech. Rev.* **39**, 511–523.

GAD-EL-HAK, M., BLACKWELDER, R. F. & RILEY, J. J. 1984 On the interaction of compliant coatings with boundary-layer flows. *J. Fluid Mech.* **140**, 257–280.

HANSEN, R. J. & HUNSTON, D. L. 1983 Fluid property effects on flow-generated waves on a compliant surface. *J. Fluid Mech.* **133**, 161–177.

HANSEN, R. J., HUNSTON, D. L., NI, C. C., REISCHMAN, M. M. & HOYT, J. W. 1979 Hydrodynamic drag and surface deformations generated by liquid flows over flexible surfaces. In *Viscous Flow Drag Reduction*; *Prog. Astro. Aero.* **72**, 439–451.

KELLER, J. B. & MUNK, W. H. 1970 Internal wave wakes of a body moving in a stratified fluid. *Phys. Fluids* **13**, 1425–1431.

KENDALL, J. M. 1970 The turbulent boundary layer over a wall with progressive waves. *J. Fluid Mech.* **14**, 259–281.

LANDAHL, M. T. 1962 On the stability of a laminar incompressible boundary layer over a flexible surface. *J. Fluid Mech.* **13**, 609–632.

LIN, J. C., WALSH, M. J. & BALASUBRAMANIAN, R. 1984 Drag of two-dimensional small-amplitude symmetric and asymmetric wavy walls in turbulent boundary layers. *NASA Tech. Paper* 2318.

MIKLOWITZ, J. 1978 *The Theory of Elastic Waves and Waveguides*. North-Holland.

PANICO, V. D. & KUBOTA, T. 1983 On the displacements generated by pressure-point advected across the surface of a viscoelastic material. *Rep.* DT-8154-05, Dynamics Technology, Inc.

SENGUPTA, T. K. & LEKOUDIS, S. G. 1985 Calculation of two-dimensional turbulent boundary layers over rigid and moving wavy surfaces. *AIAA J.* **23**, 530–536.

WILLMARTH, W. W. 1975 Structure of turbulence in boundary layers. *Adv. Appl. Mech.* **15**, 159–254.